Application of the stereographic projection to studies of magnetization dynamics described by the Landau–Lifshitz–Gilbert equation

2009 J. Phys. A: Math. Theor. 42 315211

(http://iopscience.iop.org/1751-8121/42/31/315211)

IOP PUBLISHING JOURNAL OF PHYSICS A: MATHEMATICAL AND THEORETICAL

J. Phys. A: Math. Theor. **42** (2009) 315211 (11pp) doi:10.1088/1751-8113/42/31/315211

Application of the stereographic projection to studies of magnetization dynamics described by the Landau–Lifshitz–Gilbert equation

Paul P Horley[1,2], Vítor R Vieira[1], Pedro D Sacramento[1] and Vitalii K Dugaev[1,3]

[1] Centro de Física das Interacções Fundamentais, Instituto Superior Técnico, Universidade Técnica de Lisboa, Avenida Rovisco Pais, 1049-001 Lisbon, Portugal
[2] Centro de Investigación en Materiales Avanzados S. C., Miguel de Cervantes #120, Complejo Industrial Chihuahua, CP 31109 Chihuahua, Chihuahua, Mexico
[3] Department of Physics, Rzeszów University of Technology, al. Powstańców Warszawy 6, 35-959 Rzeszów, Poland

E-mail: phorley@cfif.ist.utl.pt, vrv@cfif.ist.utl.pt, pdss@cfif.ist.utl.pt and vdugaev@prz.edu.pl

Received 15 April 2009, in final form 9 June 2009
Published 15 July 2009
Online at stacks.iop.org/JPhysA/42/315211

Abstract

We present a comparative analysis of the calculation performance for several representations of the Landau–Lifshitz–Gilbert equation (spherical, Cartesian and stereographic), underlining good perspectives to use the stereographic projection for numerical simulations of magnetization dynamics. The advantages of this approach include a five-time calculation speed-up compared to the spherical coordinate representation together with unconditional preservation of the magnetization vector length. Slightly faster calculations are achievable with the Cartesian coordinate representation, which, however, require renormalization of the magnetization vector at each integration step.

PACS numbers: 72.25.−b, 75.10.Hk, 75.60.Jk

(Some figures in this article are in colour only in the electronic version)

1. Introduction

The recent increase of interest in spintronics [1], fuelled by the successful application of the giant magnetoresistance effect [2] for the sensing heads of hard disk drives [3] and the experimental confirmation of generation of magnetization oscillations with GHz frequencies [4], attracted much attention to both theoretical and experimental studies of nanoscale magnetization dynamics. Depending on the size of the magnetic element, it can be represented by a single magnetic domain, fitting the macrospin approximation [5, 6] or will require a

complete micromagnetic treatment [7]. In either case, the temporal dynamics of an individual magnetic particle can be simulated by solving the Landau–Lifshitz–Gilbert (LLG) equation, extended with Slonczewski's spin torque term [8]

$$\frac{\mathrm{d}\vec{M}}{\mathrm{d}t} = -\gamma \vec{M} \times \vec{H} + \frac{\gamma}{M_S}\vec{M} \times (\vec{M} \times \vec{J}) + \frac{\alpha}{M_S}\vec{M} \times \frac{\mathrm{d}\vec{M}}{\mathrm{d}t}, \tag{1}$$

where $\vec{M}$ is the magnetization vector saturated with magnitude M_S,

$$\vec{H} = \vec{H}^E - (C_D M_x \vec{e}_x - C_A M_z \vec{e}_z)/M_S \tag{2}$$

is the effective magnetic field which includes the demagnetizing field defined by $C_D = M_S$ (for the case of the considered thin film), anisotropy field with coefficient $C_A = 2K_1/\mu_0 M_S$ and an external applied magnetic field $\vec{H}^E$ contributing to the energy density of the particle as $\mathcal{H}(\vec{M}, \vec{H}^E) = K_1[1 - (M_z/M_S)^2] + \frac{1}{2}\mu_0 M_x^2 - \mu_0 \vec{M} \cdot \vec{H}^E$. Quantity $\vec{J}$ is the spin-polarization vector of the injected current, $\gamma = 2.21 \times 10^5$ m A^{-1} s^{-1} is the electron gyromagnetic ratio and α is a phenomenological damping constant introduced by Gilbert [9].

Equation (1) can be rewritten in an explicit form as

$$\frac{\mathrm{d}\vec{M}}{\mathrm{d}t} = -\gamma_1 \vec{M} \times \vec{\Lambda} + \frac{\gamma_1}{M_S}\vec{M} \times (\vec{M} \times \vec{\Delta}), \tag{3}$$

with renormalized gyromagnetic ratio $\gamma_1 = \gamma/(1 + \alpha^2)$ and torque-inducing vectors

$$\vec{\Lambda} = \vec{H} + \alpha \vec{J}, \qquad \vec{\Delta} = \vec{J} - \alpha \vec{H}. \tag{4}$$

The question about the most efficient representation of the LLG equation for numerical simulations has been widely discussed. The property of the system to preserve the length of magnetization vector $\vec{M}$ naturally suggests the use of spherical coordinates, describing the magnetization evolution with azimuthal and vertical angles φ and θ, respectively [5, 6, 10]. In this way, equation (3) reduces to two ordinary differential equations

$$\begin{aligned} \frac{\mathrm{d}\theta}{\mathrm{d}t} &= \gamma_1[-\sin\varphi\Lambda_x + \cos\varphi\Lambda_y - \cos\theta(\cos\varphi\Delta_x + \sin\varphi\Delta_y) + \sin\theta\Delta_z], \\ \sin\theta\frac{\mathrm{d}\varphi}{\mathrm{d}t} &= -\gamma_1[\cos\theta(\cos\varphi\Lambda_x + \sin\varphi\Lambda_y) - \sin\theta\Lambda_z - \sin\varphi\Delta_x + \cos\varphi\Delta_y]. \end{aligned} \tag{5}$$

Despite the visual simplicity of equations (5), this system requires the calculation of trigonometric functions to obtain the value of the derivatives, effective field (2) and to reconstruct the three-dimensional behaviour of the magnetization vector as

$$\vec{M} = M_S(\cos\varphi\sin\theta, \sin\varphi\sin\theta, \cos\theta). \tag{6}$$

Such a pronounced use of trigonometric expressions, even with the advent of built-in mathematical co-processors, results in an increased calculation time.

One of the alternatives concerns the representation of equation (3) in Cartesian coordinates, which will result in a system of three ordinary differential equations

$$\begin{aligned} \frac{\mathrm{d}M_x}{\mathrm{d}t} &= -\gamma_1(M_y\Lambda_z - M_z\Lambda_y - M_x\Xi + M_S\Delta_x) \\ \frac{\mathrm{d}M_y}{\mathrm{d}t} &= -\gamma_1(M_z\Lambda_x - M_x\Lambda_z - M_y\Xi + M_S\Delta_y) \\ \frac{\mathrm{d}M_z}{\mathrm{d}t} &= -\gamma_1(M_x\Lambda_y - M_y\Lambda_x - M_z\Xi + M_S\Delta_z) \end{aligned} \tag{7}$$

with $\Xi = (\vec{M} \cdot \vec{\Delta})/M_S$.

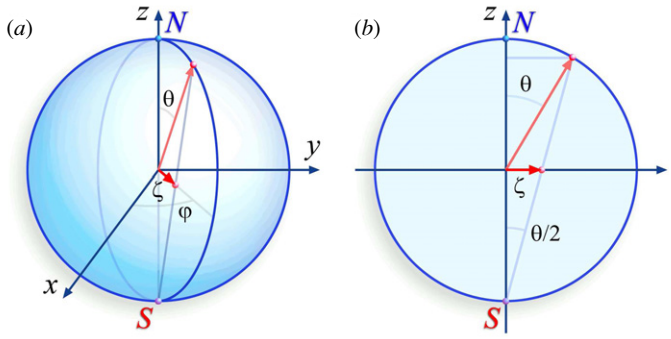

Figure 1. Stereographic projection of a point on a sphere (*a*) and definition of a complex coordinate ζ (*b*).

However, integration of system (7) does not automatically preserve the length of the magnetization vector, requiring the renormalization of $\vec{M}$ once per several integration steps. Such an approach may seem artificial and was criticized in the literature (e.g., see [11]). However, due to the total absence of trigonometric functions, it is expected to yield much faster calculation times, which may justify the extra-time involved in the renormalization of $\vec{M}$. Therefore, it is a question of extreme importance to find the optimal representation of the LLG, allowing fast numerical calculations *together* with unconditional preservation of the magnetization vector length. One of the suggested approaches concerns the use of the midpoint integration rule [11, 12], which was proved to be a reliable method conserving $|\vec{M}|$ for any reasonable step. However, midpoint integration belongs to implicit methods, applied to the original form of the LLG equation (1) with the derivatives in both left and right sides.

Here we suggest to use the stereographic projection representation of the LLG equation, which allows us to combine a simple explicit form of the system (suitable for using single-step numerical integration schemes), absence of trigonometric functions and unconditional preservation of $|\vec{M}|$.

The geometry introducing the stereographic projection is shown in figure 1. A phase point lying on a sphere with radius M_S (or $|\vec{m}| = |\vec{M}|/M_S \equiv 1$ after the conversion to dimensionless variables) can be projected to the $\{x, y\}$ plane from either the North or the South pole. The projection (figures 1(*a*) and (*b*)) from the South pole is defined by the complex variable

$$\zeta = \tan\frac{\theta}{2}\,\mathrm{e}^{\mathrm{i}\varphi} \tag{8}$$

and from the North pole by $\zeta' = 1/\zeta^*$.

Figure 2 illustrates a three-dimensional phase portrait and its stereographic projection from the South pole. As one can see, the stereographic projection allows a much clearer view (in comparison with that of a 3D plot) for the complicated structure of a single-phase trajectory connecting three stable points. In a similar way, the projections from the North and South poles can be superimposed in the same plot, offering a visual description of the system dynamics, which is simple to interpret.

As a result, using the equations from (A.19) one can write down a stereographic projection representation of the LLG equation (see the details in the appendix)

$$\begin{aligned}\frac{2}{1+\zeta^*\zeta}\frac{\mathrm{d}\zeta}{\mathrm{d}t} &= -\frac{\mathrm{i}\varsigma\gamma}{1-\mathrm{i}\varsigma\alpha}(H_{s+} - \mathrm{i}\varsigma J_{s+}) \\ &= \gamma_1[-(J_+ + i\varsigma H_+) + \alpha(H_+ - \mathrm{i}\varsigma J_+)],\end{aligned} \tag{9}$$

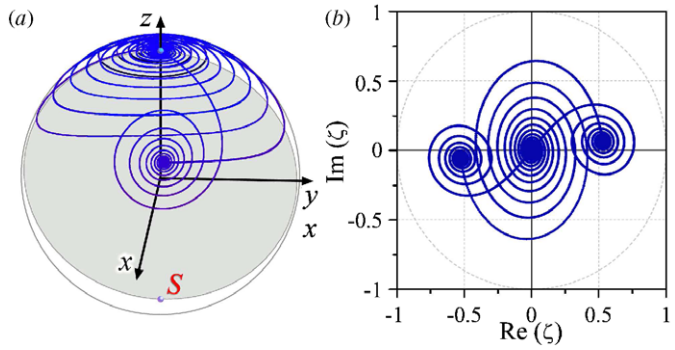

Figure 2. An illustrative phase trajectory (*a*) with the grey-filled easy magnetization plane $[y, z]$. Stereographic projection of the same trajectory (*b*) from the South pole with a unitary circle corresponding to the 'equator' $z = 0$.

introducing sign variable $\varsigma = \pm 1$ for the projection from the South and the North pole, respectively. The rotated spherical component A_{s+} of a vector $\vec{A}$ in the rotated spherical basis $\vec{b}_\pm, \vec{b}_0$ (defined in the appendix) is $A_{s+} = 2\vec{b}_+ \cdot \vec{A} = (A_+ - \zeta^2 A_- - 2\varsigma\alpha A_0)/(1 + \zeta^*\zeta)$, where $A_\pm$ and A_0 are the irreducible spherical components of a Cartesian tensor [13].

It is worth mentioning that a similar methodology could also be applied to study the evolution of quantum many-spin systems described in the framework of a coherent-state representation [14, 15].

2. Results and discussion

To test the accuracy and numerical performance of the different representations of LLG (Cartesian, spherical and stereographic), we carried out macrospin simulations for a spin valve analyser layer with dimensions $91 \times 50 \times 6$ nm^3, using material parameters of Co reported from the Co/Cu/Co spin valve experiments [4]: $\alpha = 0.014$, $C_A = 500$ Oe and $4\pi M_S = 10$ kOe. The integration of the real and imaginary parts of (9) perfectly matches the check specimen results obtained for the spherical representation of LLG (5), as illustrated in the upper panel of figure 3 for the averaged magnetization as a function of the injected spin-polarized current (circles and solid line, respectively). This figure also displays the most characteristic phase portraits (trajectories following the motion of the magnetization vector tip around the unitary sphere) for the cases of magnetization reversal (antiparallel final configuration, AP) and two steady oscillation modes (in-plane and out-of-plane precession, IPP and OPP, respectively). The bottom panels of figure 3 feature the stereographic projections of the same phase portraits. For the sake of clarity, each phase portrait was projected both from the South and North poles, yielding a superimposed picture with all the phase trajectory information contained within the unitary circle. In this way, the stereographic projection offers a convenient representation of the three-dimensional dynamic picture on a compact 2D plot. In all the cases, the initial orientation of the magnetization vector was in the vicinity of the South pole, $\vec{m} = \vec{M}/M_S = (0, 0, -0.999)$, which will correspond to the origin of the stereographic coordinates $\zeta = 0$ when projected from the North pole. To benchmark the numerical performance, we calculated the dynamical diagrams [8, 16] for the field ranges $H^E = 0 - 2$ MA m^{-1} and currents $J = 0 - 200$ mA over a 300×300 point grid. For each point, the corresponding representation of the LLG equation was integrated using the Heun method [17] with time step 0.1 ps, reconstructing the magnetization dynamics for

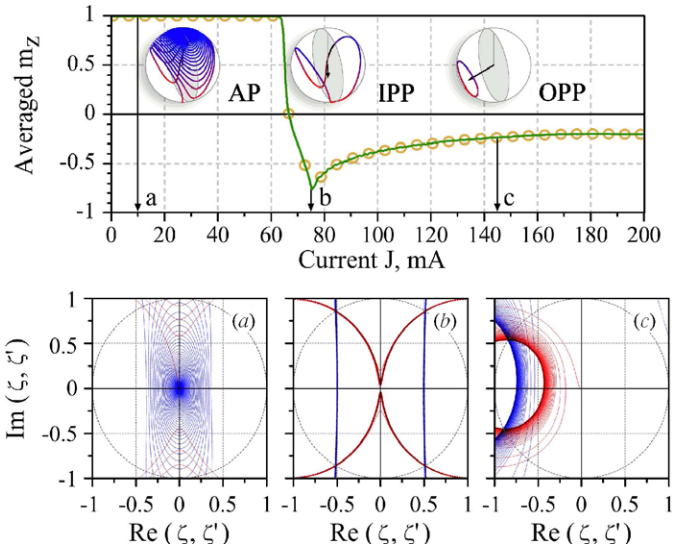

Figure 3. Upper panel: comparison of the simulation results for the LLG written in stereographic (circles) and spherical (solid line) projections, with the most characteristic phase portraits shown in 3D representation. The grey plane in the phase portraits represents the easy magnetization plane $[y, z]$ with a vertical segment corresponding to easy axis direction. The black arrow shows the averaged magnetization vector. Bottom panels: red and blue (online) or dark grey (print) contours display the same phase portraits in stereographic projection from the North and South projector poles, respectively. The phase portraits were calculated for the applied field $H = 0.35$ MA m^{-1} and injected spin-polarized currents: (*a*) 10 mA, (*b*) 75 mA and (*c*) 145 mA.

5 ns (5×10^4 points). As was anticipated, the spherical coordinate representation yielded the longest calculation time, taken as the standard for performance comparison.

For the case of the stereographic projection, special attention was paid to study numerical divergence occurring when the phase trajectory approaches the projector pole. The problem may arise if the calculations use an integration step comparable with the time constant of the system $\tau_0 = 1/(\gamma_1 C_A) \cong 114$ ps, when large values of $\mathrm{d}\zeta/\mathrm{d}t$ may cause numerical instability and overflow. To avoid such a situation, the projector pole was switched to the opposite one upon reaching a certain threshold switching value $|\zeta|_S$. The lowest threshold considered was equal to unity, requiring pole switching each time the phase trajectory crosses the equator of sphere $\theta = \pi/2$. Figure 4 shows the benchmarking curve for the stereographic projection as a function of $|\zeta|_S$. As one can see from this figure, at the threshold of 100 and above, the calculation time gravitates towards 20%, featuring an impressive five-time speed-up comparing with the spherical coordinate representation of the LLG equation. For the case of $|\zeta|_S = 10^3$, the cut-off angle inducing the pole switching will be $\theta = 0.999\,36\,\pi$, ensuring an accurate study of magnetization dynamics except for the detailed analysis of magnetization reversal. The highest threshold value displayed, $|\zeta|_S = 10^8$, is characterized with a cut-off angle equal to $0.999\,999\,9936\,\pi$, allowing us to study macrospin behaviour without the need to switch the projector pole. Even at such high values of $|\zeta|_S$, the results obtained feature a perfect fitting to the test specimen of the spherical coordinate representation of LLG, proving extremely good accuracy of the stereographic projection representation.

The black curve in figure 4 represents the calculation time for the Cartesian form of the LLG equation (6), featuring 5.9 times performance increase in comparison with the spherical

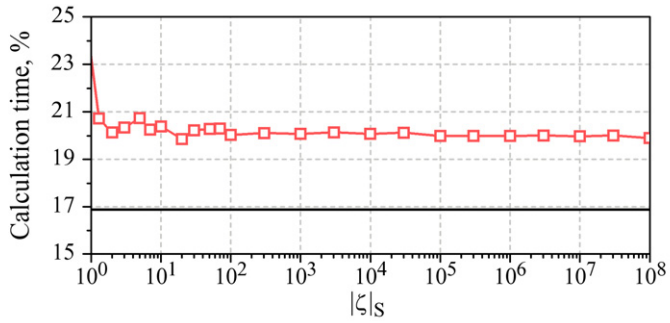

Figure 4. Comparison of calculation performance for the Cartesian (solid black line) and stereographic (squares) representations of the LLG equation as a function of the threshold value $|\zeta|_S$ after overcoming which the projector pole of the system was switched to the opposite one. The calculation time for the spherical representation of the LLG corresponds to 100%.

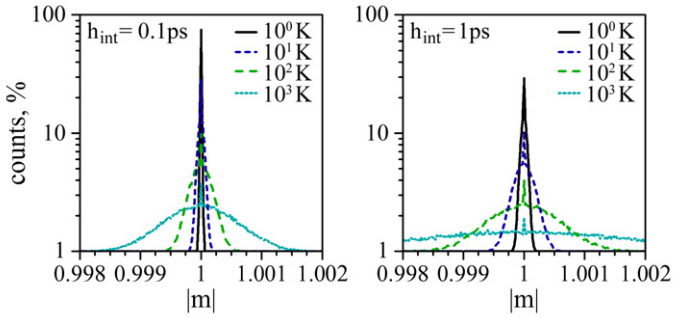

Figure 5. Distribution of vector length prior to renormalization for the case of Cartesian representation of the LLG equation, calculated for the different integration steps $h_{\rm int}$ and temperatures T.

coordinate representation. As was mentioned before, the Cartesian form does not conserve the length of the magnetization vector, therefore it was renormalized at each step to the value of unity. To justify the relevancy of renormalization, we studied the dispersion of $|\vec{m}|$ prior to the renormalization procedure for different values of the integration step and temperatures (figure 5), introduced *via* Langevin noise [18–20]. The random numbers describing the stochastic Wiener process were generated with the Ziggurat method [21].

As one can see from the figure, at $T \to 0$ the length of the magnetization vector is strictly limited to a direct vicinity of $|\vec{m}| = 1$, suggesting that renormalization does not introduce any significant changes into the behaviour of the system. Naturally, for larger values of the integration step ($h_{\rm int} = 1$ ps) the peaks of the $|\vec{m}|$ distribution become wider, leading to a significant dispersion already for $T = 10$ K. For the case of room temperatures, the tails of $|\vec{m}|$ expand beyond the interval $[0.999 - 1.001]$, jeopardizing the calculations without renormalization applied at *each* integration step. Nevertheless, the performed comparisons have shown that a renormalized Cartesian model will yield practically identical results to those obtained with the reference spherical coordinate representation. However, if one is aiming to achieve *unconditional* preservation of the magnetization vector length together with a significant increase of numerical performance, then the stereographic projection is definitely

a strong candidate for such a purpose, also offering a compact graphical representation of the three-dimensional dynamics on a complex plane.

3. Conclusions

It was shown that the use of the stereographic projection for the numerical simulations of magnetization dynamics allows us to benefit from trigonometry-free equations (ensuring fast calculations) and unconditional preservation of the magnetization vector length. The performed benchmarking revealed an impressive decrease of calculation time by a factor of 5 in comparison with the spherical coordinate representation of the system, which was considered as a control sample. This optimization is extremely important in the case of multiple-spin system simulations. In addition, the use of stereographic projection offers easy-to-interpret rendition of a phase portrait as a simple two-dimensional plot. The projection from both the North and South poles can easily be juxtaposed, giving the complete picture of magnetization dynamics in a single figure.

Moreover, similar techniques can be successfully applied to the study of general quantum many-spin systems, using a coherent-state representation.

Acknowledgments

This work was supported in part by the FCT Grants PTDC/FIS/70843/2006 and SFRH/BPD/26825/2006 in Portugal, and by the funds of the Polish Ministry of Science and Higher Education as a research project in years 2007–2010.

Appendix A

In this Appendix, we list some formulae and results which are useful when using the stereographic projection transformation.

The projection from the South pole of the unit sphere to the equatorial plane, with complex coordinate ζ, according to figures 1(*a*) and (*b*), is defined by

$$\zeta = \frac{\sin\theta}{1+\cos\theta}\,\mathrm{e}^{\mathrm{i}\varphi} = \tan\frac{\theta}{2}\,\mathrm{e}^{\mathrm{i}\varphi}. \tag{A.1}$$

The metric induced from the sphere into the equatorial plane is given by

$$\mathrm{d}\vec{s}^2 = \mathrm{d}\theta^2 + \sin^2\theta\,\mathrm{d}\varphi^2 = \frac{4|\mathrm{d}\zeta|^2}{(1+|\zeta|^2)^2}. \tag{A.2}$$

This mapping is conformal, i.e. preserves the angles between any two directions and their images at a given point.

The area (solid angle) on the equatorial plane is

$$\mathrm{d}\Omega = \sin\theta\mathrm{d}\theta\,\mathrm{d}\varphi = \frac{4\,\mathrm{d}\zeta_R\,\mathrm{d}\zeta_I}{(1+|\zeta|^2)^2}, \tag{A.3}$$

where ζ_R and ζ_I are the real and imaginary parts of ζ.

The three-dimensional unit vector $\vec{m} = \vec{r}/r = (\zeta^* + \zeta,\ \mathrm{i}(\zeta^* - \zeta), 1 - \zeta^*\zeta)/(1+\zeta^*\zeta)$ can easily be recovered from the complex variable ζ using

$$\vec{m} = \frac{\Lambda^\dagger\vec{\sigma}\,\Lambda}{\Lambda^\dagger\Lambda}, \tag{A.4}$$

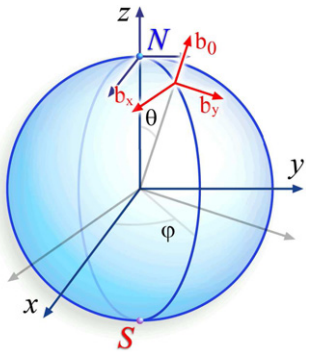

Figure A1. Fixed $[x, y, z]$ and rotated $[b_0, b_x, b_y]$ bases.

where $\Lambda(\zeta) = \binom{1}{\zeta}$ is a two-dimensional spinor with the first component equal to 1 and $\vec{\sigma}$ are the Pauli matrices. Equation (A.4) is also valid for a general spinor $\Lambda(\zeta) = \binom{\zeta_0}{\zeta_1}$ having the complex coordinate variable ζ as the homogeneous coordinate of projective geometry, i.e. $\frac{\zeta_1}{\zeta_0} = \zeta$. Under rotations, the complex variable ζ transforms according to the Möbius or fractional linear transformation homomorphic to the two-dimensional unitary transformation of the spinors. This is a geometric and probably the most straightforward manner to introduce spinors $\frac{1}{2}$ and to relate them to the usual three-dimensional vectors [22].

Similarly to the usual spherical coordinate system, with variables r, θ, φ, and basis vectors given by $\vec{e}_r = \frac{\partial \vec{r}}{\partial r}, \vec{e}_\theta = \frac{1}{r}\frac{\partial \vec{r}}{\partial \theta}, \vec{e}_\varphi = \frac{1}{r\sin\theta}\frac{\partial \vec{r}}{\partial \varphi}$, one can introduce the set of coordinates defined by r and ζ, ζ^*, considered as independent variables. The associated vectors are $\vec{m} = \vec{b}_0 = \frac{\vec{r}}{r}$ and the vectors $\vec{b}_\pm$ defined by

$$(1+\zeta^*\zeta)\frac{\partial \vec{m}}{\partial \zeta} = 2\vec{b}_-, \qquad (1+\zeta^*\zeta)\frac{\partial \vec{m}}{\partial \zeta^*} = 2\vec{b}_+. \tag{A.5}$$

They are given by

$$(\vec{b}_0 \quad \vec{b}_+ \quad \vec{b}_-) = \frac{(\vec{e}_z \quad \vec{e}_+ \quad \vec{e}_-)}{1+\zeta^*\zeta}\begin{pmatrix} 1-\zeta^*\zeta & -\zeta & -\zeta^* \\ 2\zeta^* & 1 & -(\zeta^*)^2 \\ 2\zeta & -\zeta^2 & 1 \end{pmatrix}, \tag{A.6}$$

where $\vec{e}_\pm = \frac{1}{2}(\vec{e}_x \pm \mathrm{i}\vec{e}_y)$. Figure A1 illustrates the rotated basis in terms of the vectors $\vec{b}_0, \vec{b}_x$ and $\vec{b}_y$, connected with $\vec{b}_\pm$ in the same manner as the original basis vectors $\vec{e}_x, \vec{e}_y$ and $\vec{e}_\pm$.

Vectors $\vec{b}_\pm$ are obtained from $\vec{e}_\pm$ after the rotation by angle θ around the axis $(\sin\varphi, -\cos\varphi, 0)$, converting the vector $\vec{e}_z$ into $\vec{b}_0$. This action also transforms the spin state $|J, J>$ into the coherent spin state $|\zeta>$ [14, 23, 24].

The new basis vectors are normalized

$$\vec{b}_0^2 = 1, \qquad \vec{b}_+ \cdot \vec{b}_- = \tfrac{1}{2}, \qquad \vec{b}_\pm^2 = 0, \qquad \vec{b}_0 \cdot \vec{b}_\pm = 0 \tag{A.7}$$

and properly oriented, so that

$$\vec{b}_\pm \times \vec{b}_0 = \pm\,\mathrm{i}\vec{b}_\pm, \qquad \vec{b}_- \times \vec{b}_+ = \frac{\mathrm{i}}{2}\vec{b}_0. \tag{A.8}$$

The variation of these vectors obeys

$$(1+\zeta^*\zeta)\frac{\partial}{\partial\zeta}\begin{pmatrix}\vec{b}_0\\ \vec{b}_+\\ \vec{b}_-\end{pmatrix}=\begin{pmatrix}2\vec{b}_-\\ -\vec{b}_0+\zeta^*\vec{b}_+\\ -\zeta^*\vec{b}_-\end{pmatrix}$$
$$=\ \mathrm{i}(\zeta^*\vec{b}_0+2\vec{b}_-)\times\begin{pmatrix}\vec{b}_0\\ \vec{b}_+\\ \vec{b}_-\end{pmatrix}. \tag{A.9}$$

For the sake of completeness, we summarize below some useful properties (collected from the literature or derived by the authors) for the stereographic coordinate representation. We hope this information will be useful for further research work in this field.

The differential of a point in space is given by

$$\mathrm{d}\vec{r}=\vec{b}_0\,\mathrm{d}r+\vec{b}_-\frac{2r}{1+\zeta^*\zeta}\,\mathrm{d}\zeta+\vec{b}_+\frac{2r}{1+\zeta^*\zeta}\,\mathrm{d}\zeta^*, \tag{A.10}$$

from which follows the metric on the equatorial plane, induced from the sphere, of equation (A.2). The gradient of a function is then given by

$$\nabla V=\frac{\partial V}{\partial r}\vec{b}_0+\frac{1+\zeta^*\zeta}{r}\frac{\partial V}{\partial\zeta}\vec{b}_++\frac{1+\zeta^*\zeta}{r}\frac{\partial V}{\partial\zeta^*}\vec{b}_-, \tag{A.11}$$

which can also be verified using the identity

$$\sin\theta\frac{\partial}{\partial\theta}-\mathrm{i}\frac{\partial}{\partial\varphi}=2\zeta\frac{\partial}{\partial\zeta}. \tag{A.12}$$

Similarly, the differential operations as divergence, Laplace operator and curl are given by

$$\begin{aligned}\nabla\cdot\vec{A}&=\frac{1}{r^2}\frac{\partial r^2A_r}{\partial r}+\frac{(1+\zeta^*\zeta)^2}{2r}\left[\frac{\partial}{\partial\zeta}\left(\frac{A_+}{1+\zeta^*\zeta}\right)+\frac{\partial}{\partial\zeta^*}\left(\frac{A_-}{1+\zeta^*\zeta}\right)\right]\\ \nabla^2V&=\frac{1}{r^2}\frac{\partial}{\partial r}\left(r^2\frac{\partial V}{\partial r}\right)+\frac{(1+\zeta^*\zeta)^2}{r^2}\frac{\partial^2V}{\partial\zeta\partial\zeta^*}\end{aligned} \tag{A.13}$$

$$\nabla\times\vec{A}=\frac{\mathrm{i}}{r^2}(1+|\zeta|^2)^2\begin{vmatrix}\vec{b}_0 & \frac{r}{1+|\zeta|^2}\vec{b}_+ & \frac{r}{1+|\zeta|^2}\vec{b}_-\\ \frac{\partial}{\partial r} & \frac{\partial}{\partial\zeta^*} & \frac{\partial}{\partial\zeta}\\ A_r & \frac{r}{1+|\zeta|^2}A_+ & \frac{r}{1+|\zeta|^2}A_-\end{vmatrix}. \tag{A.14}$$

The angular momentum operators $\hat{\vec{L}}=\hat{\vec{r}}\times\hat{\vec{p}}$ become

$$\begin{aligned}\hat{L}_+&=\frac{\partial}{\partial\zeta^*}+\zeta^2\frac{\partial}{\partial\zeta}\\ \hat{L}_-&=-\frac{\partial}{\partial\zeta}-(\zeta^*)^2\frac{\partial}{\partial\zeta^*}\\ \hat{L}_z&=\zeta\frac{\partial}{\partial\zeta}-\zeta^*\frac{\partial}{\partial\zeta^*}\end{aligned} \tag{A.15}$$

and the expression for operator $\hat{L}^2$ is

$$\hat{L}^2=-(1+\zeta^*\zeta)^2\frac{\partial^2}{\partial\zeta^*\partial\zeta}. \tag{A.16}$$

The extreme angular momentum spherical harmonics are expressed as

$$\begin{aligned}\phi_L^L &= (-1)^L\sqrt{\frac{2L+1}{4\pi}}\frac{\sqrt{(2L)!}}{L!}\frac{\zeta^L}{(1+\zeta^*\zeta)^L}\\ \phi_{-L}^L &= \sqrt{\frac{2L+1}{4\pi}}\frac{\sqrt{(2L)!}}{L!}\frac{(\zeta^*)^L}{(1+\zeta^*\zeta)^L}\end{aligned} \tag{A.17}$$

from which the others can be obtained using the raising and lowering operators $\hat{L}_\pm$.

Finally, the classical equation of motion

$$\frac{\mathrm{d}\vec{m}}{\mathrm{d}t} = -\vec{m}\times\vec{H} \tag{A.18}$$

becomes

$$\begin{aligned}\mathrm{i}\frac{2}{1+\zeta^*\zeta}\frac{\mathrm{d}\zeta}{\mathrm{d}t} &= H_{s+}\\ -\mathrm{i}\frac{2}{1+\zeta^*\zeta}\frac{\mathrm{d}\zeta^*}{\mathrm{d}t} &= H_{s-},\end{aligned} \tag{A.19}$$

where $H_{s\pm} = 2\vec{b}_\pm\cdot\vec{H}$ are the spherical components of vector $\vec{H} = H_+\vec{b}_- + H_-\vec{b}_+ + H_0\vec{b}_0$ in the rotated basis. Further on, if magnetic field $\vec{H}$ is obtained from a potential as $\vec{H} = -\frac{\partial\mathcal{H}}{\partial\vec{m}}$, equations (A.19) transform into

$$\begin{aligned}\mathrm{i}\frac{2}{(1+\zeta^*\zeta)^2}\frac{\mathrm{d}\zeta}{\mathrm{d}t} &= -\frac{\partial\mathcal{H}}{\partial\zeta^*}\\ -\mathrm{i}\frac{2}{(1+\zeta^*\zeta)^2}\frac{\mathrm{d}\zeta^*}{\mathrm{d}t} &= -\frac{\partial\mathcal{H}}{\partial\zeta}.\end{aligned} \tag{A.20}$$

Alternatively, these equations can be rewritten as [15, 25]

$$\begin{aligned}\frac{\mathrm{d}\zeta(t)}{\mathrm{d}t} &= \{\zeta(t), H_c\}_{PB}\\ \frac{\mathrm{d}\zeta^*(t)}{\mathrm{d}t} &= \{\zeta^*(t), H_c\}_{PB},\end{aligned} \tag{A.21}$$

where H_c is the classical Hamiltonian appropriate for the problem under consideration, and the Poisson bracket is given by

$$\begin{aligned}\{A, B\}_{PB} &= \frac{\mathrm{i}}{2J\hbar}(1+\zeta^*\zeta)^2\left(\frac{\partial A}{\partial\zeta^*}\frac{\partial B}{\partial\zeta} - \frac{\partial A}{\partial\zeta}\frac{\partial B}{\partial\zeta^*}\right)\\ &= \frac{1}{J\hbar\sin\theta}\left(\frac{\partial A}{\partial\theta}\frac{\partial B}{\partial\varphi} - \frac{\partial A}{\partial\varphi}\frac{\partial B}{\partial\theta}\right).\end{aligned} \tag{A.22}$$

Similar expressions can be obtained by projecting phase point onto stereographic plane from the North pole instead. The new complex variable is $\zeta' = \frac{1}{\zeta^*}$. Vector $\vec{m} = \vec{r}/r$ is expressed as $\vec{m} = (\zeta'^*+\zeta',\ \mathrm{i}(\zeta'^*-\zeta'), -(1-\zeta'^*\zeta'))/(1+\zeta'^*\zeta')$. Vectors $\vec{b}_\pm$ are defined as $\vec{b}_- = (\vec{e}_- - (\zeta'^*)^2\vec{e}_+ + \zeta'^*\vec{e}_0)/(1+\zeta'^*\zeta')$, $\vec{b}_+ = \vec{b}_-^*$ and a vector $\vec{b}_0 = -\vec{m}$ is defined to preserve the orientation of the basis given in equation (A.8), besides (A.7).

References

[1] Žutic I, Fabian J and Das S S 2004 Spintronics: fundamentals and applications *Rev. Mod. Phys.* **76** 323–410

[2] Baibich M N, Broto J M, Fert A, Nguyen Van Dau F, Petroff F, Eitenne P, Creuzet G, Friederich A and Chazelas J 1988 Giant magnetoresistance of (001)Fe/(001)Cr magnetic superlattices *Phys. Rev. Lett.* **61** 2472–5

[3] Kaitsu I, Inamura R, Toda J and Morita T 2006 Ultra high density perpendicular magnetic recording technologies *Fujitsu Sci. Tech. J.* **42** 122–30
[4] Kiselev S I, Sankey J C, Krivorotov I N, Emley N C, Schoelkopf R J, Buhrman R A and Ralph D C 2003 Microwave oscillations of a nanomagnet driven by a spin-polarized current *Nature* **425** 380–3
[5] Sun J Z 2000 Spin-current interaction with a monodomain magnetic body: a model study *Phys. Rev.* B **62** 570–8
[6] Xiao J, Zangwill A and Stiles M D 2005 Macrospin models of spin transfer dynamics *Phys. Rev.* B **72** 014446
[7] Berkov D V and Gorn N L 2006 Micromagnetic simulations of the magnetization precession induced by a spin-polarized current in a point-contact geometry *J. Appl. Phys.* **99** 08Q701
[8] Horley P P, Vieira V R, Gorley P M, Dugaev V K, Berakdar J and Barnas J 2008 Influence of a periodic magnetic field and spin-polarized current on the magnetic dynamics of a monodomain ferromagnet *Phys. Rev.* B **78** 054417
[9] Gilbert T L 2004 A phenomenological theory of damping in ferromagnetic materials *IEEE Trans. Magn.* **40** 3443–9
[10] Stiles M D and Miltat J 2006 Spin transfer torque and dynamics *Spin Dynamics in Confined Magnetic Structures III* (*Topics in Applied Physics* vol 101) ed B Hillebrands and A Thiaville (Berlin: Springer) pp 1–85
[11] d'Aquino M, Serpico C and Miano G 2005 Geometrical integration of Landau–Lifshitz–Gilbert equation based on the mid-point rule *J. Comput. Phys.* **209** 730–53
[12] Serpico C, Mayergoyz I D and Bertotti G 2001 Numerical technique for integration of the Landau–Lifshitz equation *J. Appl. Phys.* **89** 6991–3
[13] Normand J-M and Raynal J 1982 Relations between Cartesian and spherical components of irreducible Cartesian tensors *J. Phys. A: Math. Gen.* **15** 1437–61
[14] Vieira V R and Sacramento P D 1995 Generalized phase-space representatives of spin-J operators in terms of Bloch coherent states *Ann. Phys.* **242** 188–231
[15] Vieira V R and Sacramento P D 1995 Path integrals of spin-J systems in the holomorphic representation *Nucl. Phys.* B **448** 331–54
[16] Bazaliy Ya B, Jones B A and Zhang S-C 2004 Current-induced magnetization switching in small domains of different anisotropies *Phys. Rev.* B **69** 094421
[17] Burrage K, Burrage P M and Tian T 2004 Numerical methods for strong solutions of SDES *Proc. R. Soc. London* **460** 373–402
[18] Brown W F 1963 Thermal fluctuations of a single-domain particle *Phys. Rev.* **130** 1677–86
[19] García-Palacios J L and Lázaro F J 1998 Langevin-dynamics study of the dynamical properties of small magnetic particles *Phys. Rev.* B **58** 14937–58
[20] Chubykalo O, Hanny J D, Wongsam M, Chantrell R W and Gonzalez J M 2002 Langevin dynamic simulation of spin waves in a micromagnetic model *Phys. Rev.* B **65** 184428
[21] Marsaglia G and Tsang W W 2000 The ziggurat method for generating random variables *J. Stat. Softw.* **5** 1–7
[22] Hladik J 1999 *Spinors in Physics* (New York: Springer)
[23] Radcliffe J M 1971 Some properties of coherent spin states *J. Phys. A: Gen. Phys.* **4** 313–23
[24] Arecchi F T, Courtens E, Gilmore R and Thomas H 1972 Atomic coherent states in quantum optics *Phys. Rev.* A **6** 2211–37
[25] Kuratsuji H and Suzuki T 1980 Path integral in the representation of SU(2) coherent state and classical dynamics in a generalized phase space *J. Math. Phys.* **21** 472–6